--Supporting Information--

Exploring Ca-Ce-M-O (M = 3*d* transition metal) oxide perovskites for solar thermochemical applications

[1]Gopalakrishnan Sai Gautam, [2]Ellen B. Stechel, and [1,3,*]Emily A. Carter

[1]Department of Mechanical and Aerospace Engineering, Princeton University, Princeton, NJ 08544-5263, United States
[2]ASU Lightworks® and the School of Molecular Sciences, Arizona State University, Tempe, AZ 85287-5402, United States
[3]Office of Chancellor and Department of Chemical and Biomolecular Engineering, University of California, Los Angeles, Los Angeles, CA 90095-1405, United States
*E-mail: eac@ucla.edu

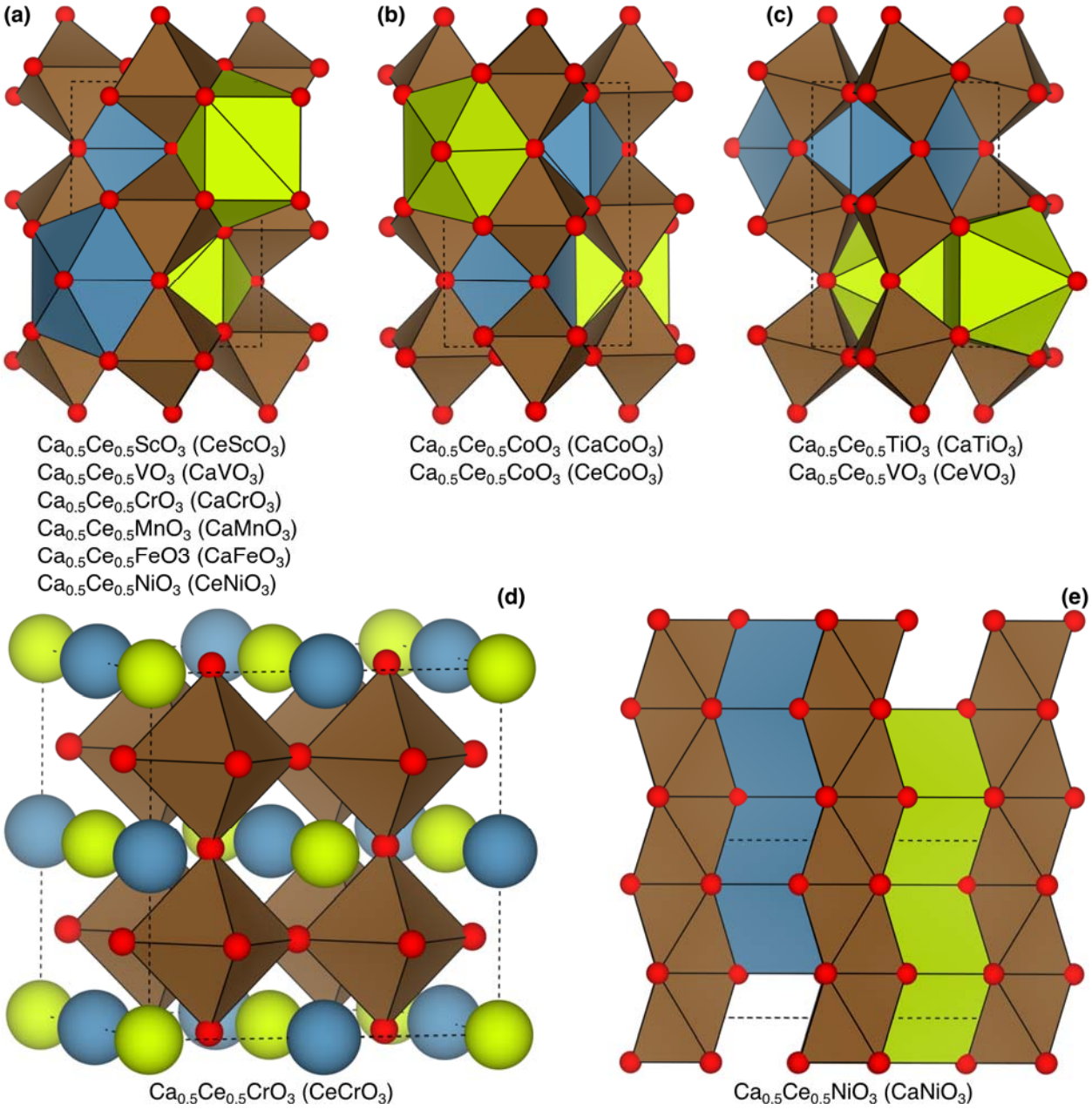

Figure S1: Initial lowest energy Ca-Ce configurations in quaternary $Ca_{0.5}Ce_{0.5}MO_3$ (M = Sc, Ti, V, Cr, Mn, Fe, Co, and Ni) perovskites considered in this work. Blue, green, brown, and red spheres or polyhedra represent Ca, Ce, M, and O, respectively. Dashed black lines in each panel highlights the unit cell. The compositions that correspond to a given Ca-Ce configuration are indicated under each structure, with the composition in brackets signifying the starting ternary perovskite. Panels (a), (b), and (c) indicate configurations based on an orthorhombic ($Pnma$) or monoclinic ($P2/c$) ternary perovskite unit cell. Both orthorhombic and monoclinic perovskites are quite similar, with the main difference being the lattice angles are not equal to 90° in the monoclinic cell. We used a $2 \times 2 \times 2$ supercell of the cubic ($Pm\bar{3}m$) $CeCrO_3$ unit cell to obtain the lowest energy Ca-Ce configuration (panel d). $Ca_{0.5}Ce_{0.5}NiO_3$ is derived from the ternary hexagonal ($P63/mmc$) $CaNiO_3$ unit cell (panel e).

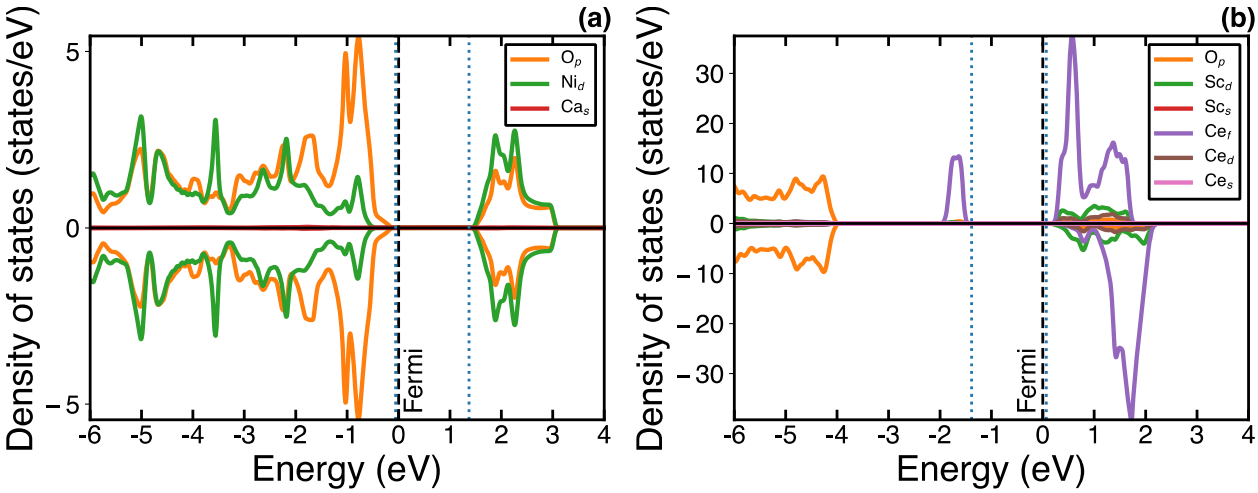

Figure S2: Projected electronic density of states (pDOS), calculated using SCAN+U, for $P63/mmc$-$CaNiO_3$ (panel a) and $Pnma$-$CeScO_3$ (panel b). Zero on the energy scale is set to the equilibrium Fermi level indicated by the dashed black lines. Dotted blue lines indicate the valence and conduction band edges. Positive (negative) values of pDOS indicate majority (minority) spin.

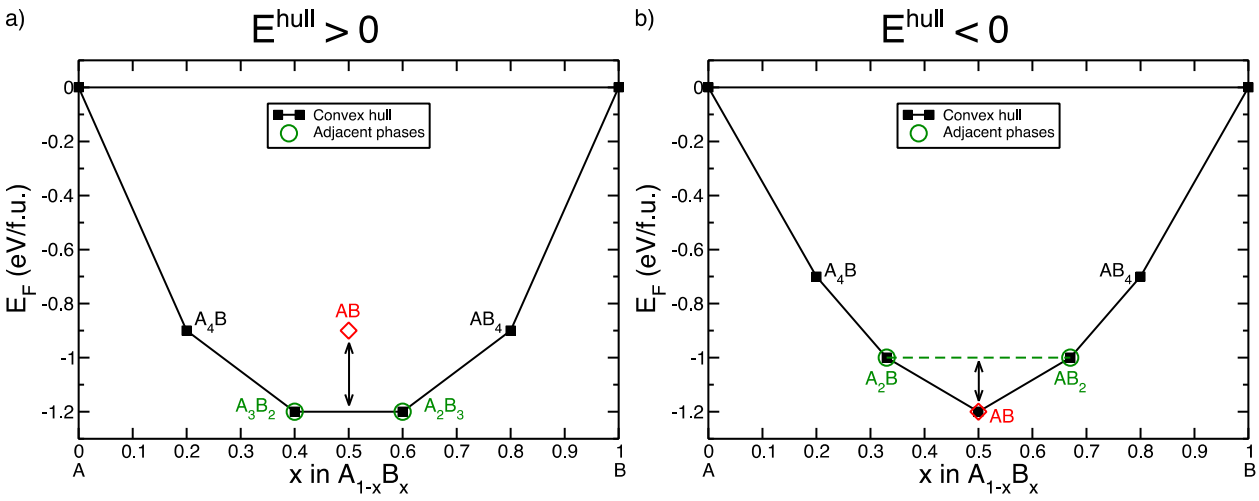

Figure S3: Schematic representation of how E^{hull} is quantified for metastable ($E^{hull} > 0$, panel a) and stable ($E^{hull} < 0$, panel b) phases in hypothetical A-B binary phase diagrams. The vertical axis is formation energy, which is defined as $E_F = E_{A_{1-x}B_x} - (1-x)E_A - xE_B$, where E_z is the Gibbs energy of species z. The convex hull in both panels is highlighted by the solid black line with the black squares signifying thermodynamically stable compounds (e.g., A_4B and AB_4). Hollow red diamond indicates the compound (AB) for which E^{hull} is defined and the hollow green circles identify the states "adjacent" to AB, namely A_3B_2+A_2B_3 in panel a and A_2B and AB_2 in panel b. Arrows indicate the magnitude of E^{hull}, which is +0.3 eV/f.u. in panel a and -0.2 eV/f.u. in panel b. Thus, E^{hull} in panel a is the largest energy release that can be obtained via decomposition of the metastable AB, while E^{hull} in panel b is the smallest energy release obtained upon formation of the stable AB.

Table S1: All states that are adjacent on the calculated 0 K convex hull to the ternary and quaternary perovksite compositions considered in this work.

Composition	Adjacent states on 0 K convex hull
Ternaries	
$CeScO_3$	$Ce_2O_3 + Sc_2O_3$
$CaTiO_3$	$Ca_4Ti_3O_{10} + TiO_2$
$CaVO_3$	$CaV_2O_4 + Ca_3V_2O_8$
$CeVO_3$	$Ce_2O_3 + V_2O_3$
$CaCrO_3$	$CaO + CaCrO_4 + CaCr_2O_4$
$CeCrO_3$	$Ce_2O_3 + Cr_2O_3$
$CaMnO_3$	$Ca_2MnO_4 + Ca_2Mn_3O_8$
$CaFeO_3$	$CaO + CaFe_2O_4 + O_2(g)$
$CaCoO_3$	$CaO + CaCo_2O_4 + O_2(g)$
$CeCoO_3$	$CeO_2 + CoO$
$CaNiO_3$	$CaO + NiO + O_2(g)$
$CeNiO_3$	$CeO_2 + NiO$
Quaternaries	
$Ca_{0.5}Ce_{0.5}ScO_3$	$CaSc_2O_4 + CeO_2$
$Ca_{0.5}Ce_{0.5}TiO_3$	$CaTiO_3 + Ce_2O_3 + Ti_2O_3$
$Ca_{0.5}Ce_{0.5}VO_3$	$CaVO_3 + CeVO_3$
$Ca_{0.5}Ce_{0.5}CrO_3$	$CaCr_2O_4 + CeO_2$
$Ca_{0.5}Ce_{0.5}MnO_3$	$CaMn_2O_4 + CeO_2$
$Ca_{0.5}Ce_{0.5}FeO_3$	$CaFe_2O_4 + CeO_2$
$Ca_{0.5}Ce_{0.5}CoO_3$	$CaCo_2O_4 + CeO_2$
$Ca_{0.5}Ce_{0.5}NiO_3$	$CaO + CeO_2 + NiO + O_2(g)$

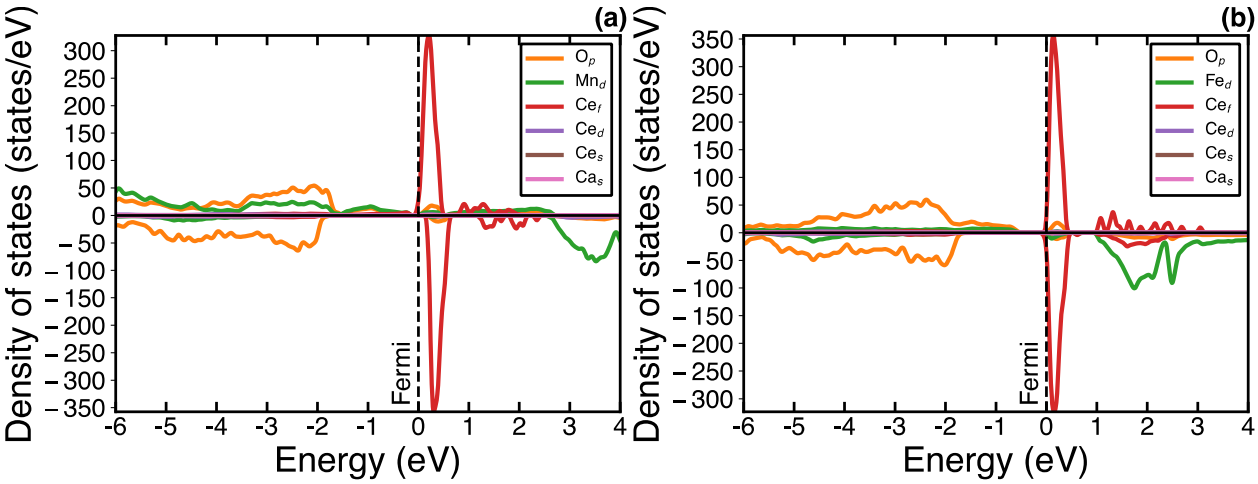

Figure S4: pDOS, calculated using SCAN+*U*, for $Ca_{0.5}Ce_{0.5}MnO_3$ (panel a) and $Ca_{0.5}Ce_{0.5}FeO_3$ (panel b) perovskites with a single oxygen vacancy. Zero on the energy scale is set to the Fermi level (dashed black line). Positive (negative) pDOS values indicate majority (minority) spin.

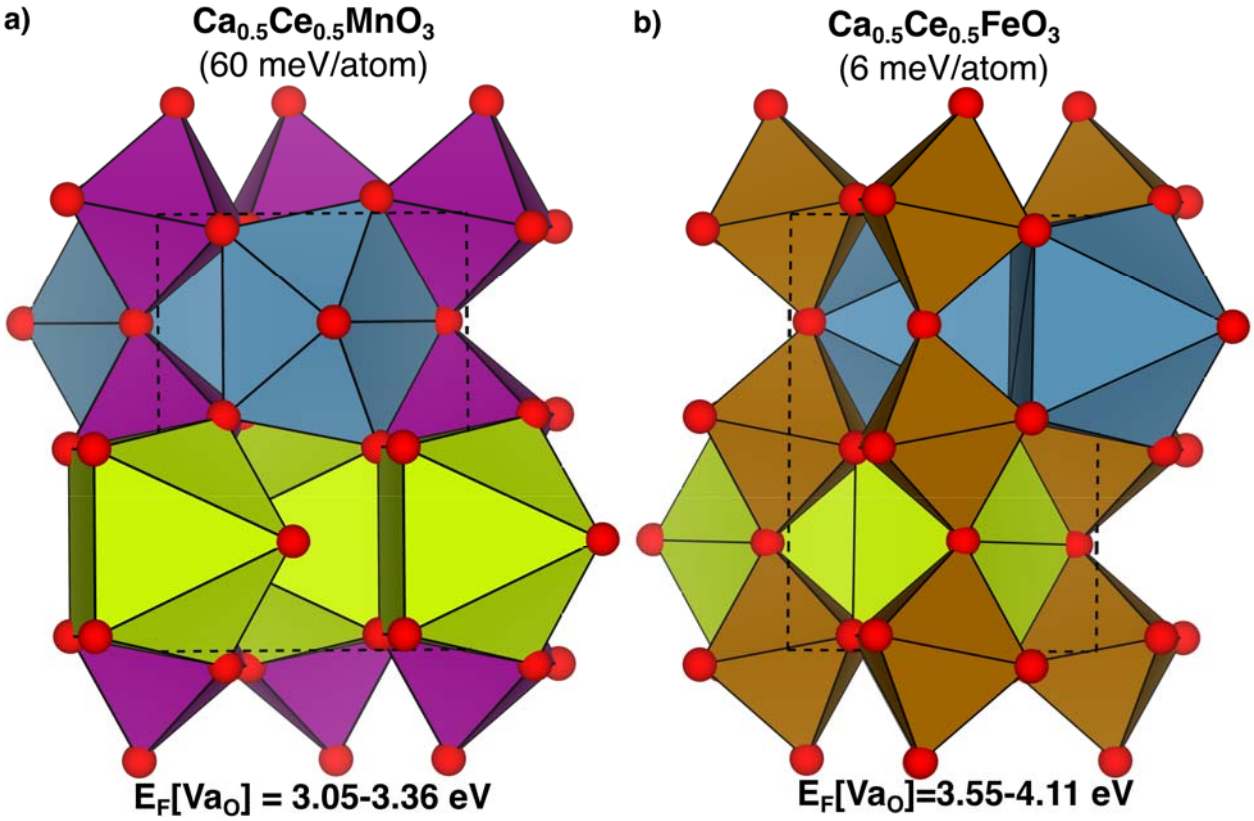

Figure S5: Initial high energy Ca-Ce configurations in $Ca_{0.5}Ce_{0.5}MnO_3$ (panel a) and $Ca_{0.5}Ce_{0.5}FeO_3$ (panel b), where the blue, olive green, purple, and brown polyhedra correspond to Ca, Ce, Mn, and Fe, respectively. Red spheres are oxygen atoms. The energy difference between the high-energy configurations displayed and the corresponding ground-state Ca-Ce configuration is indicated by the text below the structure headings. Note that the structures displayed here exhibit the highest energies amongst possible symmetrically distinct Ca-Ce configurations within the perovskite conventional 20-atom cell. The range of oxygen vacancy formation energy ($E_F[Va_O]$) for each structure is indicated by the text at the bottom in each panel, where the range is due to the symmetrically distinct oxygen vacancy configurations possible in each structure.

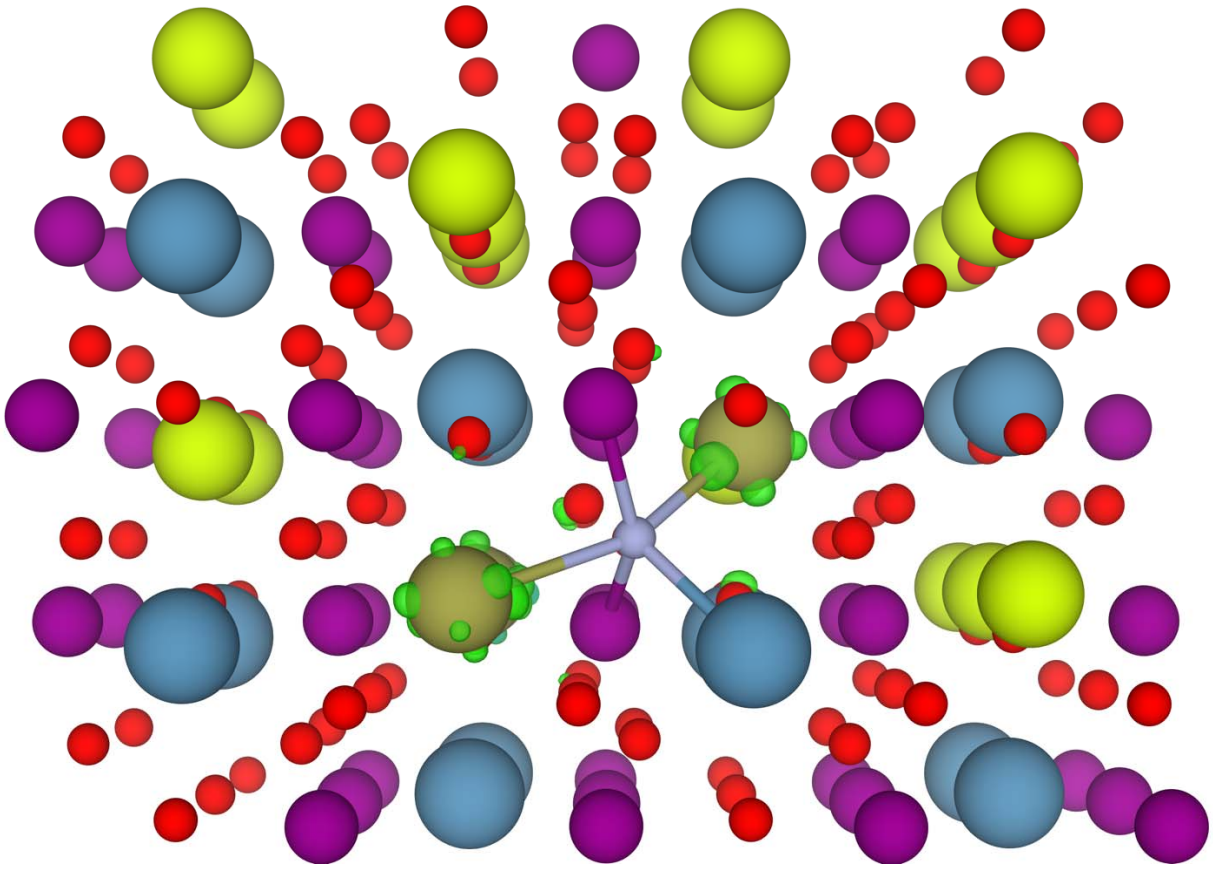

Figure S6: Electron density difference between the bulk and defective $Ca_{0.5}Ce_{0.5}FeO_3$, with the green isosurfaces (set to 0.009 e/bohr^3) representing regions of electron accumulation. Purple, blue, yellow, and red spheres are Fe^{3+}, Ca^{2+}, Ce^{4+}, and O^{2-}, respectively. The oxygen vacancy is indicated by the grey sphere with reduced Ce atoms signified by olive green spheres. The vacancy is coordinated to 2 Fe, 2 Ce, and 1 Ca atoms. The electrons created due to the oxygen vacancy accumulate on the Ce atoms that are nearest-neighbors to the vacancy and one Ce atom that is a next-nearest-neighbor, with no accumulation on any of the Fe atoms.